IEEE Access
Multidisciplinary | Rapid Review | Open Access Journal

Received February 28, 2022, accepted March 17, 2022, date of publication March 28, 2022, date of current version April 8, 2022.

Digital Object Identifier 10.1109/ACCESS.2022.3162906

An Inverter Topology for MultiTransmitter Wireless Power Transfer Systems

EKKACHAI CHAIDEE, (Member, IEEE), ANAWACH SANGSWANG, (Member, IEEE), SUMATE NAETILADDANON, (Member, IEEE), AND SUPAPONG NUTWONG

Department of Electrical Engineering, Faculty of Engineering, King Mongkut's University of Technology Thonburi, Bangkok 10140, Thailand

Corresponding author: Anawach Sangswang (anawach.san@kmutt.ac.th)

This work was supported by the Rajamangala University of Technology Lanna, Thailand.

ABSTRACT This paper presents an inverter topology for a static wireless power transfer (SWPT) system that is intended to reduce the component counts and complexity of the conventional excitation circuit for multiple transmitter coils. The proposed inverter topology requires only (n+1) power switches, where ''n'' is the number of transmitter coils. The currents in the transmitter coils can be independently controlled. The output voltage is regulated through the transmitter-side control by adjusting the duty cycle of the inverter switches. A detection method of the receiver coil position is developed by comparing the transmitter currents to the predetermined transmitter coil patterns. The proposed detection method helps decide the proper transmitter selection, which improves the transfer efficiency throughout the operation. An experimental study is performed on the created 500-watt WPT multi-coil system. As the receiver coil is placed in the designated area, the proper transmitter coil pattern can be automatically selected and energized. The output voltage can be regulated to the desired values throughout the operation, regardless of the load condition.

INDEX TERMS Inverter topology, multi-transmitter coil, transmitter-side control, output voltage regulation, receiver coil position detection, wireless power transfer.

I. INTRODUCTION

Nowadays, wireless power transfer (WPT) technique based on magnetic coupling has been adopted in various applications such as biomedical implants [1], lighting [2], mobile phone [3], kitchen appliance [4], and electric vehicle [5]. Safety, convenience, and flexible operation can be obtained from this technique due to the galvanic isolation between electrical source and load, which are the key advantages over traditional conductive power transfer.

In static wireless charging for electric vehicle (EV), the single-transmitter coil (Tx) and single-receiver coil (Rx) is commonly found [6], [7]. Both coils should be perfectly aligned to achieve high power transfer efficiency. However, misalignments between coils are inevitable in practical operation. This is the main cause of magnetic coupling variation, which resulting in the change in output voltage or output power. Moreover, power transfer efficiency is also deteriorated. Many research efforts have been introduced to address the mentioned drawbacks. An automatic frequency tracking technique was proposed to find an optimal frequency [8]–[10]. An optimal input impedance was tuned by impedance matching techniques [11], [12]. Reactive power compensation topologies with parameter optimization were reported in [13]–[15]. Magnetically coupled coil designs to achieve a uniform magnetic field were introduced in [6]. The maximum efficiency point tracking techniques to find an optimal equivalent load resistance were reported in [16], [17]. Unfortunately, these techniques are reserved for the two-coil WPT system with low misalignment tolerance.

Recently, the multi-coil WPT systems has attracted wide attentions, especially in the applications with free-positioning features. The key advantages of the multi-coil WPT system are an improvement of the power transfer efficiency and working area compared with the conventional two-coil WPT systems [18]–[21]. In this system, to determine a proper transmitter coil pattern to be excited, the knowledge of the receiver coil position is required. In [22]–[28], magnetic sensor tunneling magneto resistive (TMR) and sensing coils have been adopted to detect a receiver coil position. In [29], voltage and current profiles of the transmitter coils were used in the receiver coil detection process. This requires additional component and control, not to mention extra signal conditioner circuit to accommodate the sensors. However,

The associate editor coordinating the review of this manuscript and approving it for publication was Jiankang Zhang.

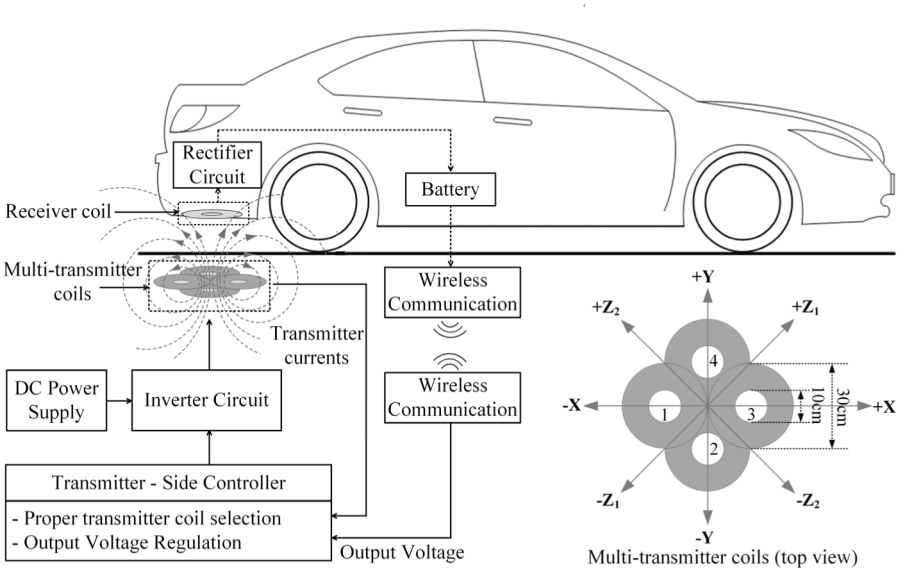

FIGURE 1. Block diagram of the proposed multi-coil SWPT system.

excitation circuits for multi-transmitter coils remain an issue in the multi-coil WPT systems. A typical multi-coil WPT system employs multiple power converters (i.e., one converter for each transmitter coil) [30]. A major drawback of this excitation is that the number of power circuit increases with the number of transmitter coils, which increases component counts, cost, and size of the system. This often yields complicated control methods. A buck-boost inverter topology with single inductor acting as a current source to drive the multi-transmitter coils was proposed in [31]. The two back-to-back MOSFETs with the body diodes have been used. This topology requires (2n+3) power switches for excitation of n transmitter coils. In [32], an inverter topology using (n+2) power switches for multi-coil WPT system was reported. The receiver coil position is detected using the additional power switches on the receiver-side. Note that these detection switches are only used during the detection process. They are turned off during normal operation. Moreover, the excitation current of each transmitter coil cannot be independently controlled.

To reduce the component counts and complexity of the conventional excitation circuits, this paper presents an improved inverter topology for multi-transmitter coil used in static WPT system. Only (n+1) power switches for n transmitter coils are required. With the proposed inverter circuit, the excitation current of each transmitter coil can be independently controlled, providing flexibility on the control aspect. Additionally, the receiver coil position can simply be detected by determining the transmitter current, without any external circuit or sensor. The DC output voltage is regulated through the duty cycle of the inverter's switches.

The benefit of the proposed inverter is twofold: reduced number of required switches and independent current control. For n-transmitter coils, the proposed inverter requires only n+1 power switches, compared with 4n switches of a conventional full-bridge inverter. The component count and the switching loss are lower in the proposed work. In addition, each transmitter current can be arbitrarily set to accommodate the desired charging profile since the excitation current can be independently controlled through the corresponding duty cycle of the gate signal.

The paper is organized as follows: The proposed system is described in Section II. The magnetic profile is analyzed in section III. The circuit configuration, timing diagram, and mode of operation of the proposed inverter topology are detailed in Section IV. The proposed circuit is analyzed in section V. The proper transmitter coils selection method is explained in Section VI. The transmitter-side controller is outlined in Section VII. Experimental validation of the proposed system is presented in Section VIII. Section VIX concludes this work.

II. SYSTEM DESCRIPTIONS

Block diagram of the proposed static wireless power transfer (SWPT) system with multiple transmitter coils is presented in Figure 1. The main components consist of DC voltage source for supplying dc power to the inverter circuit. The proposed (n+1) inverter circuit is used to convert DC power to high-frequency AC power. The presented multi-transmitter coils are deployed and arranged in a double-layer coil configuration, as shown in Figure 1. The overlap between coils increases the mutual flux. Each coil is aligned to fill as much of the square-shaped working area as possible. With this structure, the receiver coil can move freely within the designated area with slightly decreased coupling factor. This increases the misalignment tolerance of the system. A maximum horizontal distance in the z direction is equal to the radius of a receiver coil. To achieve this coil arrangement, four identical coils are adopted as the multi-transmitter pad. Each coil is in circular shape comprising 32 turns of litz wire.

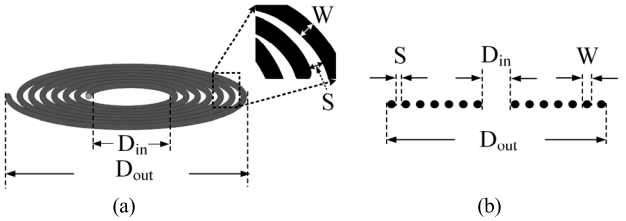

FIGURE 2. Physical representation of planar spiral coil (a) planar spiral coil (b) cross-section view.

The inner and outer diameters are 10 and 30 cm, respectively. The Rx coil has the same dimension as the Tx coils. Note that the receiver can be moved up to 30 cm in x and y directions from the center of the transmitter pad. In the z direction, it can be moved up to 15 cm. The double-layer multi-transmitter coil configuration, commonly found in portable wireless chargers [33], [34]. The number of activated transmitter coils is properly assigned corresponding to the receiver position to ensure maximum power transfer efficiency.

A. INDUCTANCE CALCULATION

Figure 2 shows the coil configuration as a planar spiral inductor. The coil outer and inner diameters are denoted D_{out} and D_{in}, respectively. S is the space between each turn, while N is the number of turns and W is the wire diameter. The inductance formula based on the mentioned physical dimension in Figure 2 can be derived as

$$L = \frac{N^2 (D_{out} + D_{in})^2}{20.32\,(15D_{out} - 7D_{in})} \tag{1}$$

The relationship between D_{out} and D_{in} is given by

$$D_{out} = D_{in} + 2W + (2\mathrm{N} - 1)(S + W) \tag{2}$$

The fabrication of each transmitter coil can be created from the above relationship. Considering the area of a typical wireless charging pad for EVs, D_{out} of each Tx coil and the receiver coil are all set to 30 cm. S is set to the minimum possible value, since an extra space between turns would reduce the mutual inductance and results in lower transfer efficiency. In a typical design process, the parameters S, W and D_{out} are fixed. The desired coil inductance in micro Henry is obtained by adjusting D_{in} and N as mentioned earlier in (1) and (2).

III. ANALYSIS OF THE MAGNETIC PROFILE

The finite element analysis (FEA) of the magnetic profile of two sets of coupled coils used in a static wireless power transfer system is introduced in this section. The simulation studies are conducted via COMSOL Multiphysics. For comparison purpose, two different geometry of transmitter (Tx) coils are coupled with the same receiver (Rx) coil, as shown in Figure 3. A single transmitter coil having an identical dimension to a receiver coil is presented in Figure 3(a). Multi-transmitter coils are shown in Figure 3(b). The diameter of each Tx coil is equal to the receiver coil. Simulation results of the magnetic flux distribution are shown in Figure 4. In both

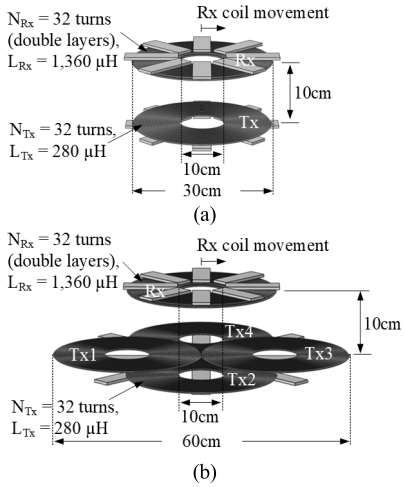

FIGURE 3. Two geometry of the transmitter coils (a) single transmitter coil (b) multi-transmitter coils.

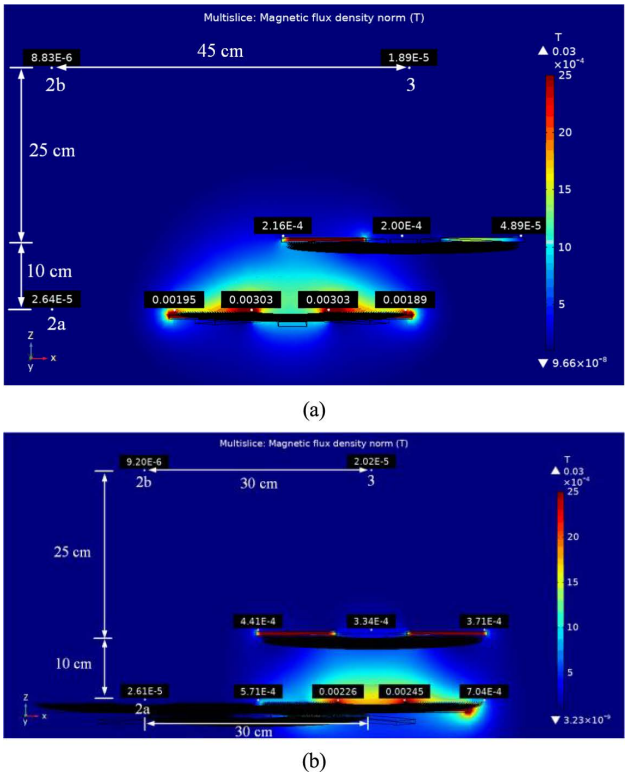

FIGURE 4. The magnetic flux distribution under lateral misalignment (a) single transmitter coil (b) Multi-transmitter coils.

cases, the air gap is fixed at 10 cm and the receiver coil is placed at 15 cm away from the center of the transmitter coil pad (15 cm lateral misalignment). In figure 4(a), the lowest mutual flux linkage between Tx and Rx coils has occurred. The lateral misalignment causes a considerable amount of leakage flux, which has virtually no contribution to the power transfer. The magnetic flux density at the center of the Rx coil is 200 μT. The highest mutual flux is obtained in the case of multi-transmitter coils, as shown in Figure 4(b). The leakage flux becomes very low, while the magnetic coupling between Tx and Rx coils has been improved. At the same

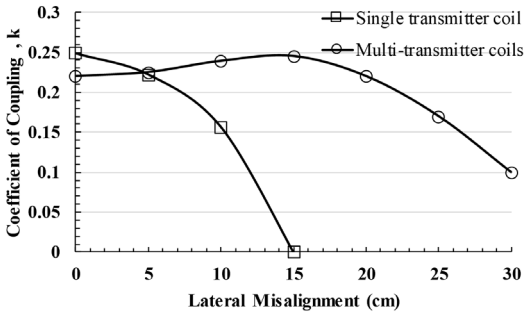

FIGURE 5. Comparison of the magnetic coupling coefficient under lateral misalignment between two studied cases.

point as the case of the single-transmitter coil, the magnetic flux density at the center of the Rx coil increases to 334 μT. Furthermore, the magnetic flux densities, at the test points, 2a, 2b, and 3, within the test region in SAE J2954 [35] have to comply with the ICRNP2010 [36], as shown in figure 4. The values of magnetic flux density in both cases, at points 2a are 26.4 μT and 26.1 μT, at points 2b are 8.83 μT and 9.20 μT and at points 3 are 18.9 μT and 20.2 μT for the single-transmitter and multi-transmitter coils, respectively. Clearly, the magnetic flux densities at all points do not exceed the limit value of 27 μT according to recommend in ICNIRP2010 [36].

A comparison of the magnetic coupling coefficient between both studied cases when the receiver coil is placed in the area between 0 to 30 cm from the center of the transmitter coil pad (0 to 30 cm lateral misalignment) is shown in Figure 5. At zero misalignment, the magnetic coupling in the case of a single transmitter coil is higher than the multi-transmitter coil. However, in the single transmitter coil, the magnetic coupling is drastically decreased as the misalignment is increased. This is due to the weak mutual flux and strong leakage flux. Note that a larger single-transmitter pad offers a similar coupling coefficient characteristic in between the single-transmitter coil and the multi-transmitter coil systems. To construct a larger single-transmitter pad with the same coverage area would require a similar amount of copper and ferrites to the multi-transmitter configuration, with significantly lower transfer efficiency. In the case of multi-transmitter coils, the magnetic coupling is at the highest value at 15 cm of lateral misalignment. The magnetic coupling is then decreased in the same manner as the single transmitter coil but with the lower steepness. This results in higher power transfer efficiency compared with the single transmitter.

IV. INVERTER TOPOLOGY

This paper presents an inverter topology for a static wireless power transfer (SWPT) system that is intended to reduce the component counts and complexity of the conventional excitation circuit for multiple transmitter coils. In practice, the misalignment exists when a receiver coil is located away from the transmitter coil. This is the case when an EV arrives at the charging post. The magnetic coupling is decreased as the misalignment between coupled coil increases and the charging efficiency is the price to pay. In multi-coil configuration, the activated transmitter coil can be properly selected with respect to the receiver position.By turning on only the tightly coupling transmitter coil, the misalignment tolerance of the system can be improved. The proposed circuit configuration of the multi-coil WPT system is represented in Figure 6. The inverter circuit consists of (n+1) MOSFET switches for the excitation of n transmitter coils. The switches S_1 to S_n with the corresponding antiparallel diodes D_{S1} to D_{Sn} are used to control the excitation of the transmitter coils. The lower switch S_L with its antiparallel diode D_{SL} works in a complementary manner to S_1 to S_n. The diodes D_{b1} to D_{bn} block undesired currents while the diodes D_{f1} to D_{fn} act as freewheeling diodes. L_{t1} to L_{tn} are the self-inductance of each transmitter coil. C_{t1} to C_{tn} are compensation capacitors, which connected in series with each transmitter coil. Lr and C_r are the self-inductance of the receiver coil and compensation capacitor, respectively. The series resonant circuits on both sides form the series-series compensation topology. This system starts with the conversion of a dc input voltage (V_{dc}) to a high-frequency alternating voltage V_{t1} to V_{tn}. The high-frequency current I_{ti} flows into transmitter coils to generate magnetic flux coupling between coils. The voltage V_{rc} and current I_{rc} are generated and converted to the dc output voltage V_{out} and current I_{out} by the rectifier circuit. The transmitter current of each coil is sensed to the transmitter-side controller to detect the receiver coil position and determine a proper excitation of transmitter coils. The dc output voltage is measured and sent to the transmitter-side controller via wireless communication to regulate the output voltage. This can be done by adjusting the duty cycle, known as pulse width modulation (PWM) technique, of the gate signals of the excitation switches V_{gs1} to V_{gsn}. The lower switch S_L is controlled by the gate signal V_{gsL}, which has fixed duty cycle of 50%. This signal lags gate signals of the excitation switches by 180 degrees to ensure safety operation. Different duty cycles of the gate signal can be assigned to drive the power switches. Therefore, the excitation current of each transmitter coil can be independently controlled. Since the proposed topology requires only n+1 power switches, in the two-coil (1-Tx, 1-Rx) system, the number of required switches is 2. For the proposed configuration, the number of switches becomes 5, compared with 16 in the full-bridge topology. The switching loss is evidently reduced.

A. MODE OF OPERATION

Operation of the proposed inverter circuit in each mode is explained in this part. Timing diagram and corresponding waveforms of the transmitter-side circuit is shown in Figure 7. For illustrative purposes, transmitter coils 1 and 3 are used as an example of the proposed independent transmitter coil control. The power switches S_1, S_3, and S_L are driven by the corresponding gate signals with the duty cycles of 50%, 35%, and 50%, respectively. The switching frequency is intentionally set at a slightly higher value than the resonant frequency so that the inverter operates under inductive mode.Therefore,

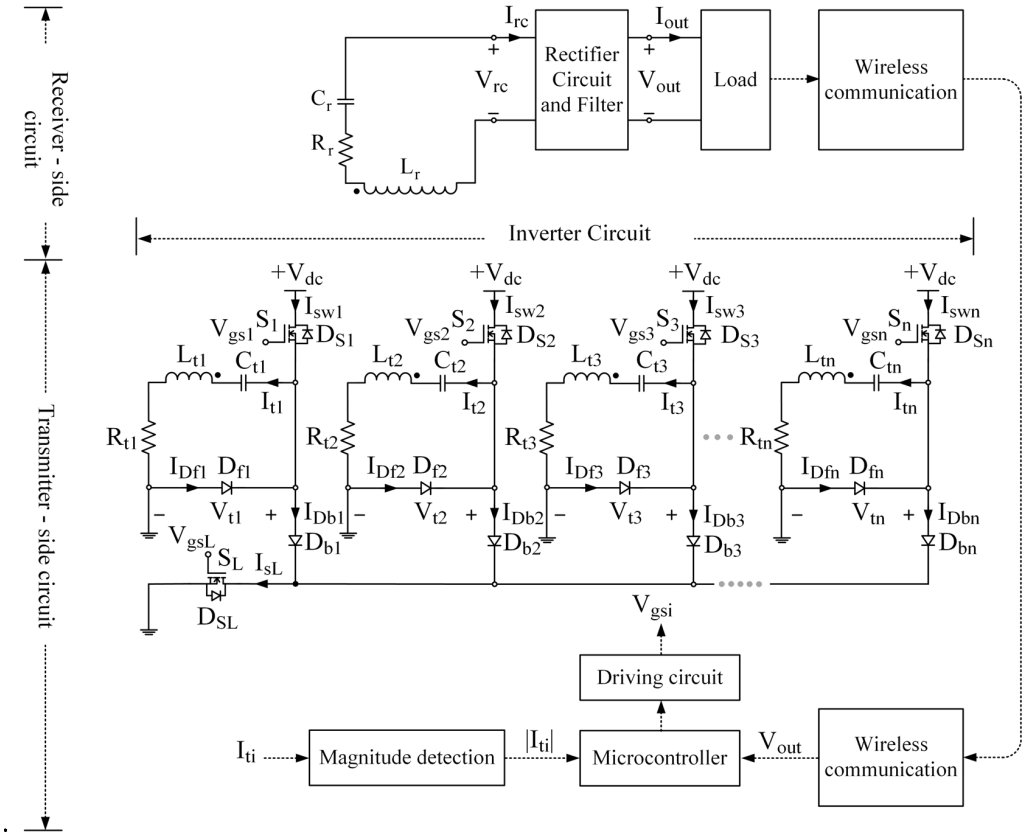

FIGURE 6. The proposed circuit configuration.

the ZVS operation is inherently achieved. For each switching period, the modes of operation are divided into seven modes. The resulting circuit of each mode is presented in Figure 8. For simplicity, all power switches and diodes are assumed to be ideal, and the dead-time between the upper and lower switch is neglected. All operation modes in Figure 7 are explained as follows:

1) MODE 1 (t_0 - t_1)

The gate signals V_{gs1} and V_{gs3} are active while the switch S_L is turned off. The negative currents I_{t1} and I_{t3} flow through anti-parallel diodes D_{s1} and D_{s3}, respectively. The inverter voltages V_{t1} and V_{t3} are equal to the dc input voltage V_{dc}. The transmitter current I_{t1} and I_{t3} lag the output voltages due to the inductive behavior of the circuit.

2) MODE 2 (t_1 - t_2)

The gate signals V_{gs1} and V_{gs3} are still active, and the switch S_L remains off. The switch S_3 conducts positive current I_{t3} while the voltage V_{sw3} is zero. The ZVS operation is achieved. The transmitter current I_{t1} is still negative. The phase difference between the currents I_{t1} and I_{t3} is due to different duty cycles of the switches S_1 and S_3.

3) MODE 3 (t_2 - t_3)

While the switch S_L is off, the switch S_1 starts conducting positive current I_{t1}. The inverter voltage V_{t1} and V_{t3} are equal to the dc input voltage V_{dc}. The switch S_1 operates under ZVS mode.

4) MODE 4 (t_3 - t_4)

Gate signal of the switch S_3 is changed from positive value to zero at t_3 where the switch starts to turn off. The lower switch S_L remains off, while the switch S_1 is still on. The inverter voltage V_{t1} is equal to V_{dc}, but the inverter voltage V_{t3} becomes zero. The positive transmitter current I_{t1} keeps on flowing through the switch S_1. The transmitter current I_{t3} still flows in a positive direction through the freewheeling diode D_{f3}.

5) MODE 5 (t_4 - t_5)

Gate signal of the switch S_1 is changed from positive value to zero at t_4. At the same time, gate signal of the lower switch S_L is shifted from zero to positive value. The switch S_1 and S_3 are turned off, but the lower switch S_L is turned on. The inverter voltage V_{t1} and V_{t3} are equal to zero. The transmitter current I_{t1} still flows in a positive direction through a freewheeling diode D_{f1}. The transmitter current I_{t3} does not change direction and reduce to zero at t_5.

6) MODE 6 (t_5 - t_6)

In this mode, switches S_1 and S_3 are still off. The lower switch S_L remains on. The inverter voltage V_{t1} and V_{t3} are equal to zero. The transmitter current I_{t3} starts flowing in a

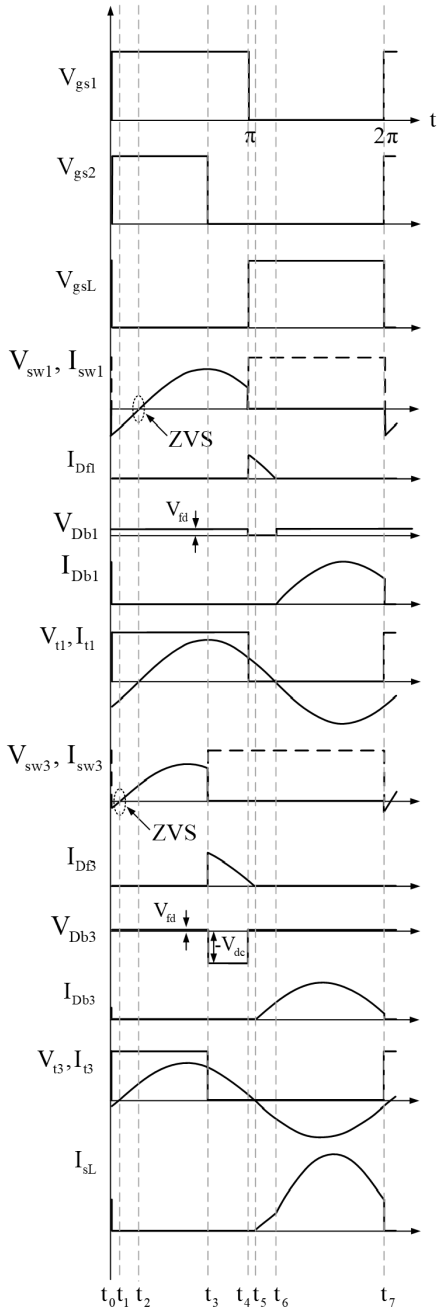

FIGURE 7. Timing diagram and corresponding waveforms of transmitter-side circuit.

negative direction at t_5 through the blocking diode D_{b3} and the lower switch S_L. The positive transmitter current I_{t1} still flows through the freewheeling diode D_{f1}.

7) MODE 7 (t_6 - t_7)

This mode is defined as the end of the switching operation. The switches S_1 and S_3 are still off. The lower switch S_L remains on. The inverter voltage V_{t1} and V_{t3} are equal to zero. The transmitter current I_{t1} starts flowing in a negative direction at t_6 through the blocking diode D_{b1} and the lower switch S_L. The transmitter current I_{t3} does not change direction. Furthermore, in case of the two transmitter coils are activated at the same time, the current from the activated coil cannot flow through the other activated coil because they are blocked by the blocking diode in each transmitter circuit. Considering the resulting circuit in figure 8(g), both diodes D_{b1} and D_{b3} conduced the I_{Db1} and I_{Db3}, respectively. Since they are forwarded conduction equipment, the proposed circuit offers no current path for the activated transmitter current to flow to or even interact with other transmitter currents. The operation of one switching period is completed at t_7. The switching operation is then repeated starting from mode 1.

V. CIRCUIT ANALYSIS

The equivalent circuit of the proposed multi-coil SWPT system is shown in Figure 9. The winding resistances of the transmitter coils and receiver coil are represented by R_{t1} to R_{tn} and R_r, respectively. The equivalent ac load resistance [37] are denoted by,

$$R_{Leq} = \frac{8R_L}{\pi^2} \tag{3}$$

where R_L is the DC load resistance. ω is the angular frequency. The mutual inductance between the transmitter coils is neglected since it is considerably low compared with the mutual inductance between the transmitter and receiver coils (M_{tnr}). The relationship between voltages and currents can be derived as,

$$\begin{bmatrix} I_{t1} \\ I_{t2} \\ \vdots \\ I_{tn} \\ I_r \end{bmatrix} = \begin{bmatrix} Z_{t1} & 0 & \cdots & 0 & j\omega M_{t1r} \\ 0 & Z_{t2} & \cdots & 0 & j\omega M_{t2r} \\ \vdots & \vdots & \ddots & \vdots & \vdots \\ 0 & 0 & \cdots & Z_{tn} & j\omega M_{tnr} \\ j\omega M_{t1r} & j\omega M_{t2r} & \cdots & j\omega M_{tnr} & Z_r \end{bmatrix}^{-1} \times \begin{bmatrix} V_{t1} \\ V_{t2} \\ \vdots \\ V_{tn} \\ 0 \end{bmatrix} \tag{4}$$

where $Z_{t1} = R_{t1} + j(\omega L_{t1} - 1/\omega C_{t1})$, $Z_{t2} = R_{t2} + j(\omega L_{t2} - 1/\omega C_{t2})$, .. $Z_{tn} = R_{tn} + j(\omega L_{tn} - 1/\omega C_{tn})$, and $Z_r = R_r + R_{Leq} + j(\omega L_r - 1/\omega C_r)$

Using the fundamental harmonic approximation (FHA), the fundamental component of the inverter voltage V_{t1} to V_{tn} can be obtained by V_{ti}^1 where its amplitude can be derived as,

$$\left|\overrightarrow{V_{ti}}^1\right| = \frac{V_{dc}}{\pi}\sqrt{2 - 2\cos(2\pi D)} \tag{5}$$

where V_{dc} is the dc input voltage and D is the duty cycle of the gate signals of the excitation switches. The output voltage and output power are given by,

$$V_{out} = \frac{\sum_{i=1}^{n} (j\omega M_{tir} I_{ti}) R_{Leq}}{\left[(R_r + R_{Leq}) + j\left(\omega L_r - \frac{1}{\omega C_r}\right)\right]} \tag{6}$$

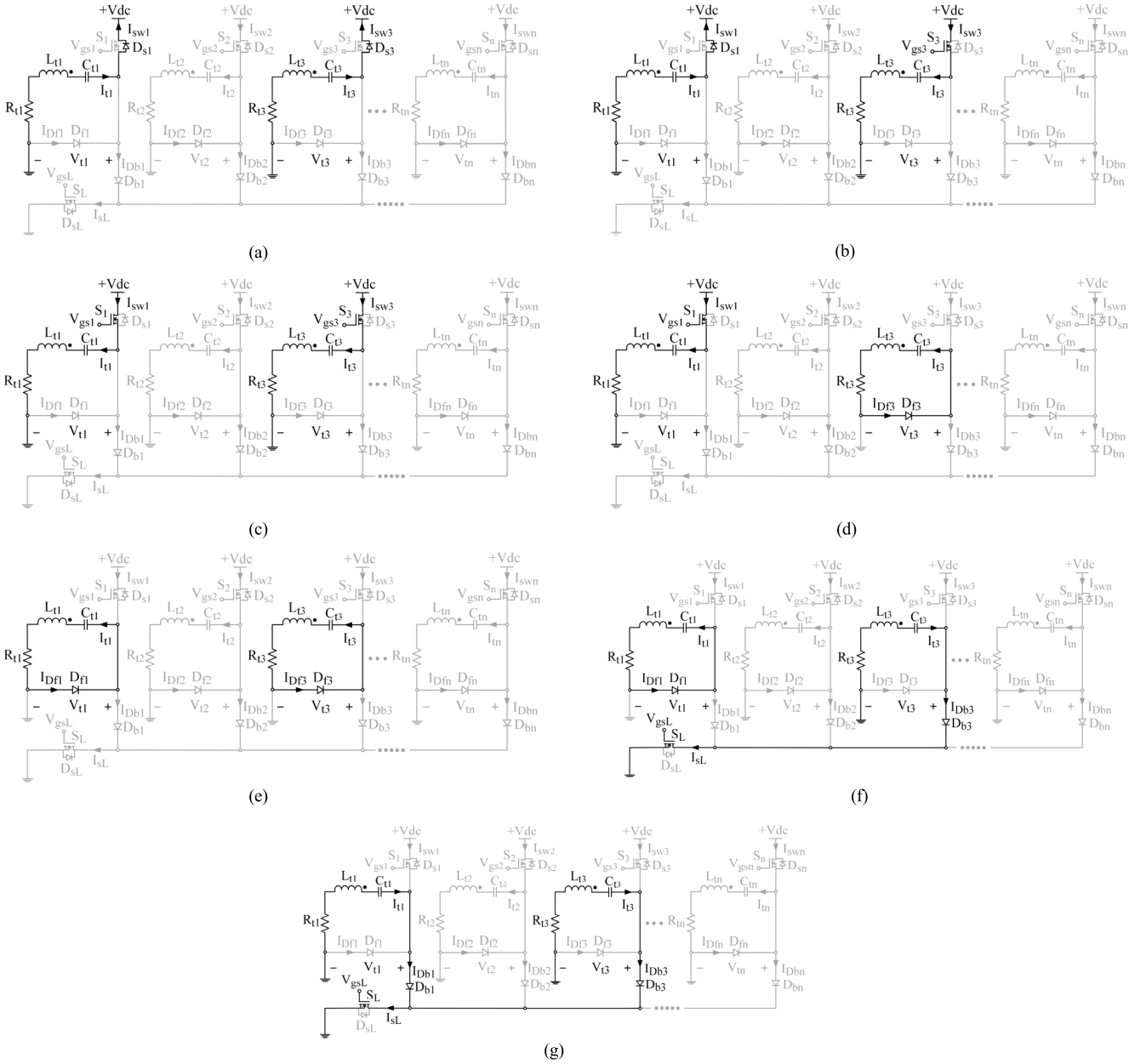

FIGURE 8. Mode of operations: (a) Mode 1 (t_0-t_1); (b) Mode 2 (t_1-t_2) (c) Mode 3 (t_2-t_3) (d) Mode 4 (t_3-t_4) (e) Mode 5 (t_4-t_5) (f) Mode 6 (t_5-t_6) (g) Mode 7 (t_6-t_7).

$$P_{out} = \frac{\left[\sum_{i=1}^{n} (j\omega M_{tir} I_{ti})\right]^2 R_{Leq}}{\left[(R_r + R_{Leq}) + j\left(\omega L_r - \frac{1}{\omega C_r}\right)\right]^2} \tag{7}$$

From (4) and (5), the output voltage (V_{out}) and output power (P_{out}) can be regulated by adjusting the duty cycle of the gate signals (V_{gs1} to V_{gsn}). The power transfer efficiency is calculated from,

$$\eta = \frac{|I_r|^2 R_{Leq}}{\sum_{i=1}^{n} \left(|I_{ti}|^2 R_{ti}\right) + |I_r|^2 \left(R_r + R_{Leq}\right)} \tag{8}$$

For a given output power, the efficiency is decreased as the transmitter current is increased. Therefore, the weakly coupled coil will consume higher current compared with the tightly coupled coil, for the same amount of transferred power. Turning it off can help improve efficiency. To correctly determine the set of Tx coils to be energized, the receiver coil position must be properly detected.

VI. EXCITATION OF THE PROPER TRANSMITTER COIL

A. DETECTION OF THE MAGNETIC COUPLING COEFFICIENT

The key advantage of the multi-transmitter coil SWPT system is the improvement of power transfer efficiency under

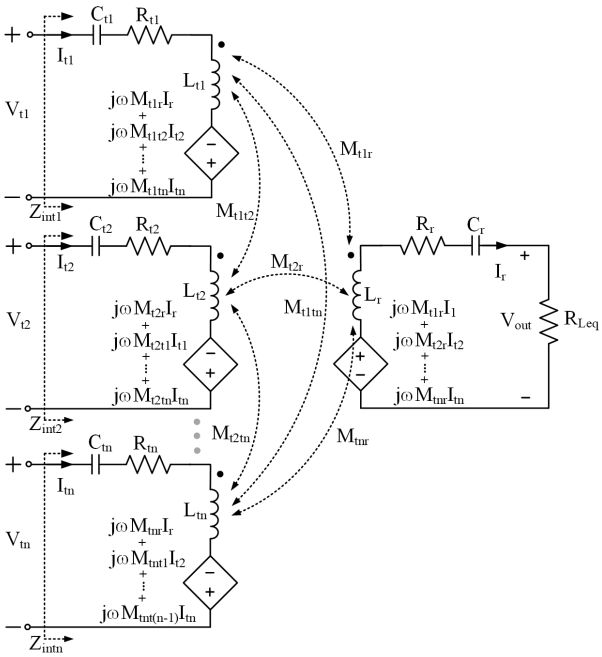

FIGURE 9. Equivalent circuit of the proposed multi-coil SWPT system.

lateral misalignment. The free-positioning feature, where the receiver coil can be moved freely in the designated area, is possible through the magnetic coupling with one or more transmitter coils at a time. The transmitter coil set with tight coupling to the receiver coil should be identified. On the other hand, an activation of weakly coupled coils should be avoided, to maintain the charging efficiency. Therefore, the detection method to differentiate the tightly coupled coils from loosely coupled ones is proposed based on the measured current obtained from each transmitter coil. The current pattern of the transmitter coil with respect to the receiver coil position is analyzed for the coupling boundary. As the predetermined coupling boundary and the corresponding current values are established, the proper transmitter coils can be identified and energized.

The relationship between transmitter current magnitude and magnetic coupling coefficient of the two-coil SWPT system is derived as,

$$\left|\overrightarrow{I_{ti}}\right| = \frac{(V_{dc}/\pi)\sqrt{2-2\cos(2\pi D)}}{\sqrt{\left[R_{ti}+\frac{(\omega k\sqrt{L_{ti}L_r})^2(R_r+R_{Leq})}{(R_r+R_{Leq})^2+X_r^2}\right]^2+\left[X_{ti}-\frac{X_r(\omega k\sqrt{L_{ti}L_r})^2}{(R_r+R_{Leq})^2+X_r^2}\right]^2}} \tag{9}$$

where, $X_{ti} = (\omega L_{ti} - 1/\omega C_{ti})$, $X_r = (\omega L_r - 1/\omega C_r)$. From (9), if the receiver coil is moved away from the transmitter coil, the transmitter current will increase. This is due to the incremental of the misalignment where the magnetic coupling is decreased. To detect the receiver coil position, the magnetic coupling between each transmitter and the receiver coil is determined. Since the transmitter and receiver coils are

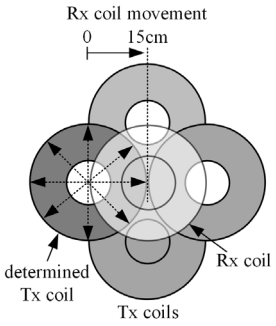

FIGURE 10. Coupling boundary of a multi-transmitter system with respect to the receiver coil movement.

circular, the magnetic coupling between both coils is radial symmetry [6]. The same current pattern of the transmitter coils are observed as the receiver coil is moved from the center of a transmitter coil (0 cm) to the outer radius of a transmitter coil (15 cm), regardless of the direction, as shown in Figure 10. Figure 11 shows the measured magnetic coupling coefficient and transmitter current magnitude with respect to the receiver coil position. When the receiver coil is horizontally moved away from the perfectly aligned position at 0 cm to 20 cm, the magnetic coupling is monotonically decreased, whereas the current magnitude is increased in agreement with the expression in (9). When the receiver coil position is greater than 15 cm, the outer radius of transmitter coils, the magnetic coupling decreases drastically. The receiver coil is now under the influence of the adjacent transmitter coils, as observed in Figure 10. Thus, the magnetic coupling at the outer radius of the transmitter coil (15 cm) is selected as the coupling boundary (k_{bound}). In this setup, the k_{bound} value is 0.08 with the corresponding measured transmitter current of 2.6 A is defined as the boundary current (I_{bound}). Note that the error between the calculated and measured boundary currents is at 3.8 percent. The transmitter coil with the magnetic coupling lower than k_{bound} is classified as weakly coupled coil, which can be detected by comparing the measured transmitter current with the I_{bound} current. The proposed transmitter coil selection method and output voltage regulation can be extended to arbitrary movement of the receiver coil in the space, specifically in the vertical direction. Since the effect of a varied position of the receiver, regardless of the direction, would result in a change in the coupling and the proposed detection can be used to identify a proper set of transmitters to activated.

B. SELECTION OF THE PROPER TRANSMITTER COIL

The process to select the proper transmitter coil to be excited, with respect to the position of the receiver coil, are as follows: First, the transmitter coil is energized, one at a time. Each Tx coil current is then compared with the I_{bound} (2.6 A). If it is less than or equal to the I_{bound}, it means the magnetic coupling is greater than or equal to the k_{bound}, which can be considered as tightly coupled. Thus, the Tx coil will be excited. To demonstrate the selection process at various receiver coil

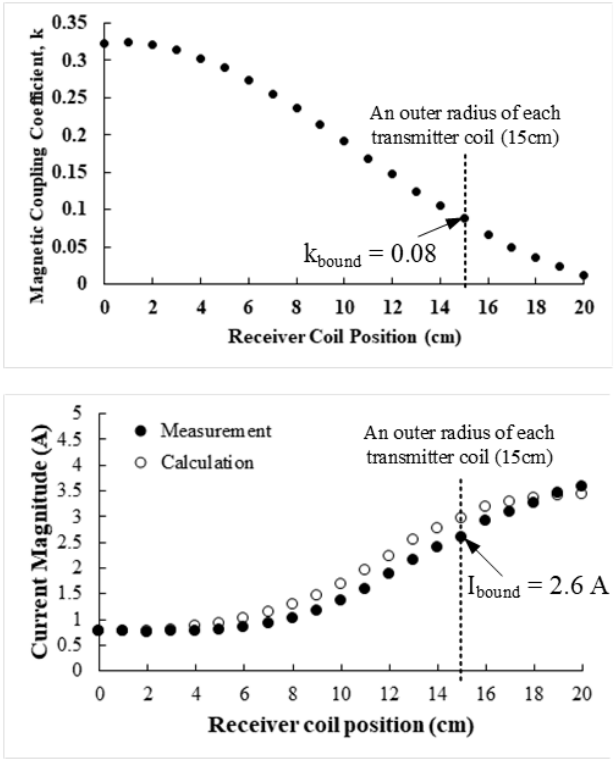

FIGURE 11. Measurement of magnetic coupling coefficient and the current magnitude of each transmitter coil when a receiver coil is horizontally moved from the center of each Tx coil (0 cm) to 20 cm.

positions, the current magnitude of each transmitter coil is measured as the receiver coil is moved from the center of Tx coil 1, as shown in Figure 12 and 13. After comparing these measured currents with the I_{bound}, the proper transmitter coil to be energized will be obtained. As considered in Figure 12, only Tx coil 1 will be selected to excite if the receiver coil position is in the range between the center of Tx coil 1 (0 cm) and 10 cm. This is due to the measured current of the Tx coil 1 is lower than the I_{bound} (2.6 A). The Tx coils 1, 2 and 4 will be excited, if the receiver coil is moved in the range between 11 and 14 cm from the center of the Tx coil 1. At 15 cm, all Tx coils will be excited since the receiver coil is placed at the radius of all transmitter coils where all transmitter currents are equal to the I_{bound}. For the movement of the receiver coil in the direction as shown in Figure 13, only the Tx coil 1 will be selected to excite when the receiver coil position is in the range between the center of the Tx coil 1 (0 cm) and 4 cm. The Tx coils 1 and 4 will be selected to excite, if the receiver coil is located in the range between 5 and 15 cm from the center of the Tx coil 1. After the detection process of the receiver coil position, two or more transmitter coils may be activated if the receiver coil is located at the position under their influence.For example, when a receiver coil is located between Tx coils 3 and 4, both coils are excited.The cross-coupling between transmitter coils may be observed. However, the currents in both coils are set proportionally with respect to the position of the receiver.It may be substantially lower compared with the single activated

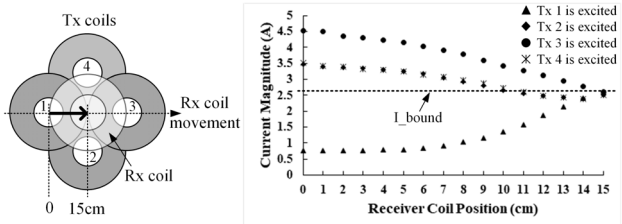

FIGURE 12. Demonstration of the selection process when a receiver coil is horizontally moved from the center of Tx coil 1 toward Tx coil 3.

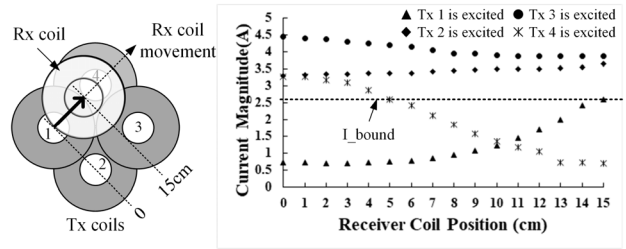

FIGURE 13. Demonstration of the selection process when a receiver coil is horizontally moved from the center of Tx coil 1 toward Tx coil 4.

Tx coil, so as the cross-coupling between transmitter coils. Since all transmitter coils are aligned in the same plane, so the magnetic coupling is relatively low compared with the main coupling between transmitter and receiver coil in the vertical direction.The cross-coupling effect on the inactive coils is negligible because the inserted free-wheeling diode in each transmitter circuit allows the circulated current to flow in the positive direction only. Therefore, the effect of the cross-coupling between transmitter coils is disregarded in this work.

VII. TRANSMITTER-SIDE CONTROL

The output voltage regulation is essential in WPT systems since the output voltage may deviate from the desired value when the load or the mutual inductance between coupled coils is changed. In this work, the output voltage control is implemented on the transmitter-side, which can be done by adjusting the duty cycle of the inverter switch. The transmitter-side controller operates in two modes, transmitter coil selection and output voltage regulation. The operation of both modes has been illustrated in the block diagrams as shown in Figure 14. The working procedures of the transmitter-side control is shown in Figure 15. The transmitter coil selection mode in Figure 14(a) is detailed as follows: First, each transmitter coil is energized at a time, for the purpose of current measurement. The transmitter current (I_{ti}) is sensed using a current transformer and fed to the magnitude detector, as shown in Figure 14(a). It is then converted to digital through the ADC converter. The estimated current is essentially instantaneous and used in the current control throughout the charging process and in the receiver detection process at the beginning by comparing the transmitter current magnitude with the boundary current, as described earlier.

After completing the transmitter coil selection process, the proper transmitter coils are excited. The controller then

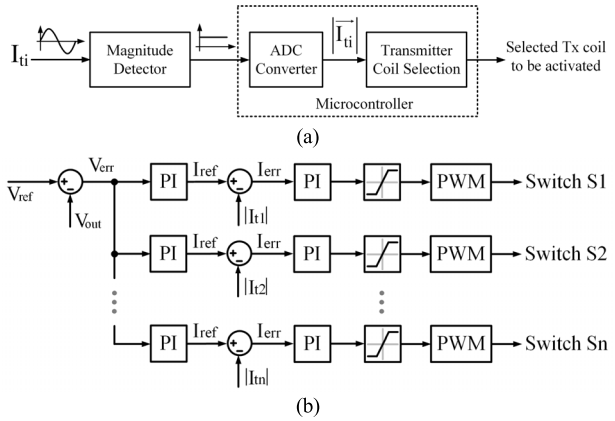

FIGURE 14. Block diagram of the transmitter-side controller: (a) the transmitter coil selection mode (b) output voltage regulation mode.

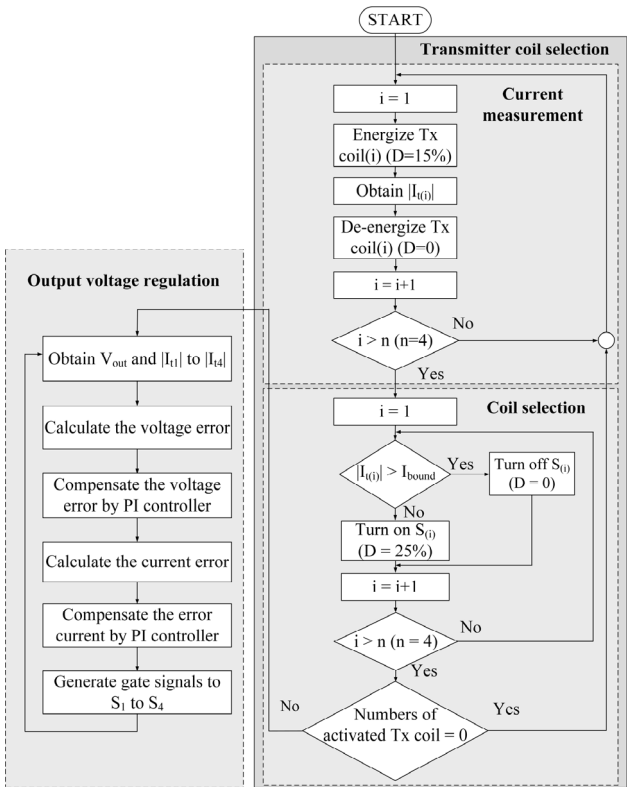

FIGURE 15. Flowchart of the transmitter-side controller.

operates in the output-voltage regulation mode, as shown in Figure 14(b). The outer control loop is the voltage control whereas the inner control loop is the current control. The output voltage is measured and wirelessly sent to the transmitter-side controller. This voltage will be compared with the reference voltage (V_{ref}) in the outer voltage control loop. The error is passed to the PI controller where the reference transmitter current (I_{ref}) needed to regulate the output voltage is obtained at the PI output. The current will then be compared with the measured transmitter current in the inner current loop. The duty cycle command for the gate signal of the inverter's switch is then obtained. Since the measured current of each Tx coil depends on the receiver coil position, the obtained error from each Tx coil current comparison may be different. The error obtained from the Tx coil with tight coupling is greater than ones with loosely coupled. This is due to the inverse relationship between transmitter current and the magnetic coupling in (9). The duty cycle command from the PI output is directly proportional to the magnetic coupling between the transmitter coil and a receiver coil. The main inverter's switches for each Tx coil current control can be operated independently. A proper current sharing between excited Tx coils is therefore possible with the proposed method.

The flowchart of the transmitter-side controller is shown in Figure 15. First, the controller operates in the current measurement process. Four transmitter coils (n = 4) are energized one by one. To avoid excessive current in the transmitter coils, duty cycle (D) of the excitation switches S_1 to S_4 are assigned at 15 percent. Each transmitter current is measured by the current transformer and fed to the magnitude detector, as detailed in Figure 14(a). All measured Tx currents magnitude are sent to the controller. After the controller read these currents, the magnitude of all transmitter currents ($|I_{t(1)}|$-$|I_{t(4)}|$) will be obtained. Then, the controller will operate in the proper transmitter coils selection process. The measured magnitude of all transmitter currents $|I_{t(1)}|$-$|I_{t(4)}|$ are compared with the boundary current (I_{bound}), which is set to 2.6 A. If they are greater than I_{bound}, the corresponding switches S_1 to S_4 will be turned off (D = 0%) to deactivate the transmitter coils. In contrast, if they are lower than I_{bound}, the corresponding switches S_1 to S_4 will be turned on with 25% duty cycle to activate the transmitter coils. Next, the controller will check the number of activated Tx coils. If none of the coil is activated, it means that all Tx coils are not sufficiently coupled with the receiver coil. The controller will repeat the operation starting from the current measurement process. On the other hands, if the number of activated Tx coils are not zero, the control will enter the output voltage regulation process. Once the output voltage is measured, it is wirelessly sent to the transmitter side. The controller will read this output voltage as well as the transmitter current magnitude ($|I_{t(1)}|$-$|I_{t(4)}|$). Then, the obtained voltage will compare with the reference voltage. The voltage error is compensated by the PI controller and used as the reference Tx coil current, as described in Figure 14(b). This reference current will compare with the obtained Tx coil current magnitude. After compensated the current error by the PI controller, the duty cycle command for the gate signal of switches S_1 to S_4 will be achieved. The generated PWM signals are fed to the corresponding switches. Note that the proposed transmitter coil selection method and output voltage regulation can be extended to arbitrary movement of a receiver coil in the space, including vertical direction. This is due to any receiver coil position in space can be detected through the presented transmitter current comparison.

VIII. EXPERIMENTAL RESULTS

To validate the proposed multi-coil SWPT system, a 500 W, laboratory prototype is created as shown in Figure 16.

It consists of a dc power supply, the proposed inverter circuit, four transmitter coils, a receiver coil, compensation capacitors, rectifier circuit, and a resistive load. The proposed control strategy is implemented on TMS320F283379D microcontroller unit. The circular magnetic structure is adopted for the coupled coil. According to the minimum ground clearance of EVs, air gap between transmitter and receiver coil is set to 10 cm. Considering the area of typical wireless charging pad for EVs, outer diameter of each Tx coil and a receiver coil are selected to be 30 cm. The receiver coil is constructed as a double-layer configuration to make up for the desired output voltage, so the self-inductance is approximately 5 times of the transmitter inductance. The inner diameter and number of turns of the coils are adjusted to obtain desired magnetic coupling, which can be achieved using FEA simulation. To reduce leakage flux, ferrite cores are included in both transmitter and receiver coils. The measured self-inductance and winding resistance of the coupled coil are listed in Table 1. Considering the voltage and current rating of the power switch used in the inverter circuit, the switching frequency is appointed as 60 kHz. Capacitance of the compensation capacitors are calculated with respect to the coil inductance to form a series resonant circuit. DC input voltage is set to 150 V to comply with the 110 V electrical system. Load resistance is chosen according to the output voltage and rated power of the created experimental setup. In the proposed multi-coil SWPT system, the transmitter coils are fixed, while the receiver coil can be laterally moved in a designated area.

First, the experimental measurement of the proposed system is performed. All Tx coils are excited all together. The receiver coil is placed at the outer radius of each Tx coils which is the center of the multi-transmitter coil pad, as shown in Figure 17(a). The 35% duty cycle of the gate signal is assigned to the selection switches S_1 to S_4. The duty cycle of the lower switch S_L is set at 50%. Experimental waveforms are shown in Figure 18. The measured inverter voltage and current of the Tx coil 1 are shown in Figure 18 (a). The waveforms are in good agreement with the theoretical waveforms as described in section IV. In Figure 18(b), the measured current in the Tx coil is essentially identical in both magnitude and phase. This is due to the magnetic coupling between each Tx coil and the receiver coil is almost the same. The measurement of the receiver-side circuit is shown in Figure 18(c). From the measured DC output voltage and current, the output power is at 500 W.

Next, an experimental measurement of the system under the proper transmitter coil selection process is performed. The receiver coil is placed between the transmitter coils 1 and 4, as shown Figure 17(b). One of the transmitter coils is energized at a time. The 15% duty cycle of the gate signal is assigned to all selection switches S_1 to S_4. The 50% duty cycle is set to the lower switch S_L. The measured magnitude of all transmitter currents are shown in Figure 19. The current magnitude of the transmitter coils 2 and 3 (I_{t2} and I_{t3}) are greater than the I_{bound}. This indicates that the receiver coil

TABLE 1. Circuit parameters of the proposed system.

Parameters	Symbol	Value
Self-inductance of the transmitter coil	$L_{t1} - L_{t4}$	280 μH
Self-inductance of the receiver coil	L_r	1,360 μH
Winding resistance of transmitter coil	$R_{t1} - R_{t4}$	0.33 Ω
Winding resistance of receiver coil	R_r	2.03 Ω
Load resistance	R_L	100 Ω-150 Ω
Transmitter compensation capacitance	$C_{t1} - C_{t4}$	25.2 nF
Receiver compensation capacitance	C_r	5.2 nF
Filter capacitance	C_f	560 μF
Switching frequency	f	60 kHz
Input voltage	V_{dc}	150 V

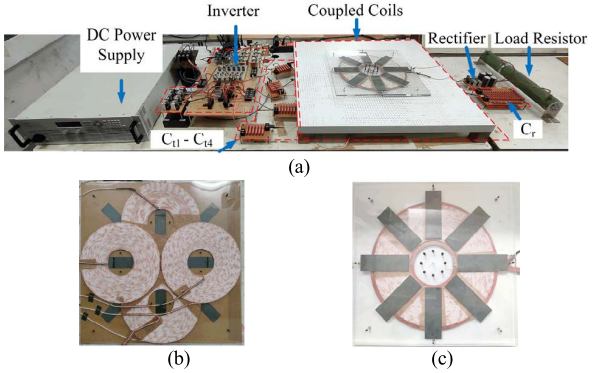

FIGURE 16. Experimental setup of the proposed system: (a) overall system; (b) four transmitter coils with double-layer configuration; (c) single receiver coil.

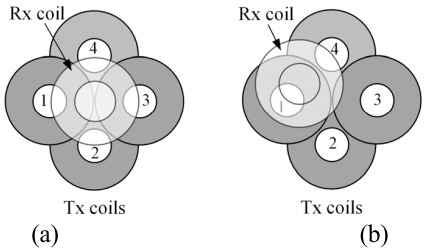

FIGURE 17. A receiver coil is placed (a) at the center of the multi-transmitter coil pad (b) between Tx1 and Tx4.

is located far away from the Tx coils, since the magnetic coupling is lower than the k_{bound}. The excitation switches S_2 and S_3 will be turned off. Alternatively, the measured current magnitudes of transmitter coils 1 and 4 (I_{t1} and I_{t4}) are lower than the I_{bound}. This indicates that the receiver coil is placed near the Tx coils where the magnetic coupling is higher than the k_{bound}. Therefore, both excitation switches S_1 and S_4 will be turned on. The current I_{t4} is very close to the I_{bound} since the receiver coil is located approximately at the outer diameter of Tx coil 4. The measured inverter voltage and current of the Tx coil 4 is illustrated in Figure 19.

The output voltage regulation of the proposed transmitter-side control is experimentally verified under load changes. The receiver coil is placed at the position shown in

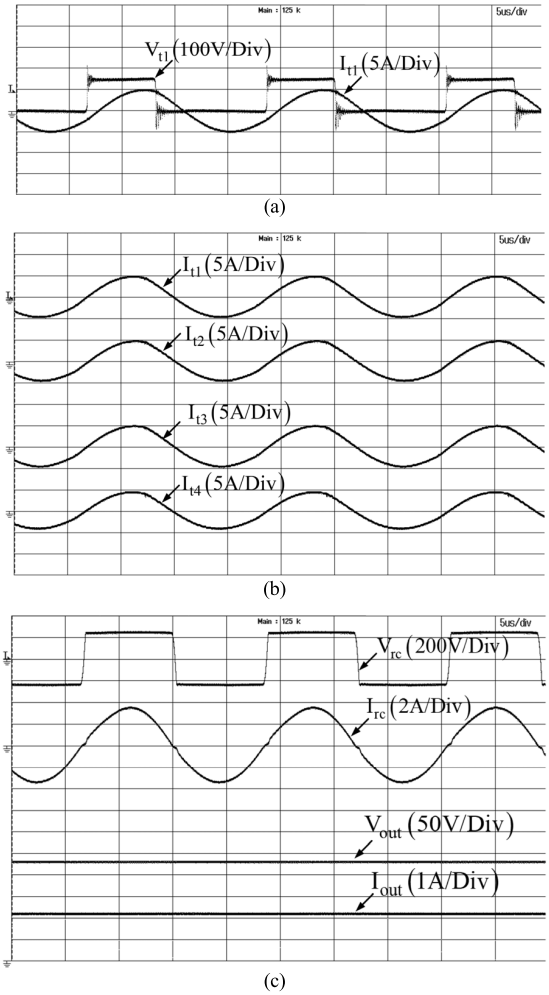

FIGURE 18. Experimental waveforms when all transmitter coils are selected to excite; (a) inverter voltage (V_{t1}) and current in transmitter coil 1 (I_{t1}); (b) Current in each transmitter coil ($I_{t1} - I_{t4}$); (c) Rectifier input voltage (V_{rc}), rectifier input current (I_{rc}), dc output voltage (V_{out}), and dc output current (I_{out}).

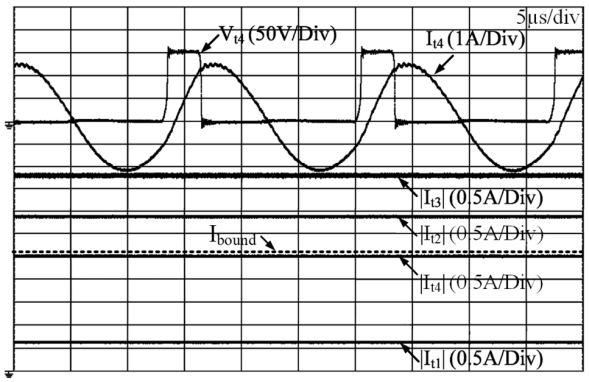

FIGURE 19. Experimental waveforms of the system under transmitter coil selection mode when the receiver coil is placed between transmitter coil 1 and 4.

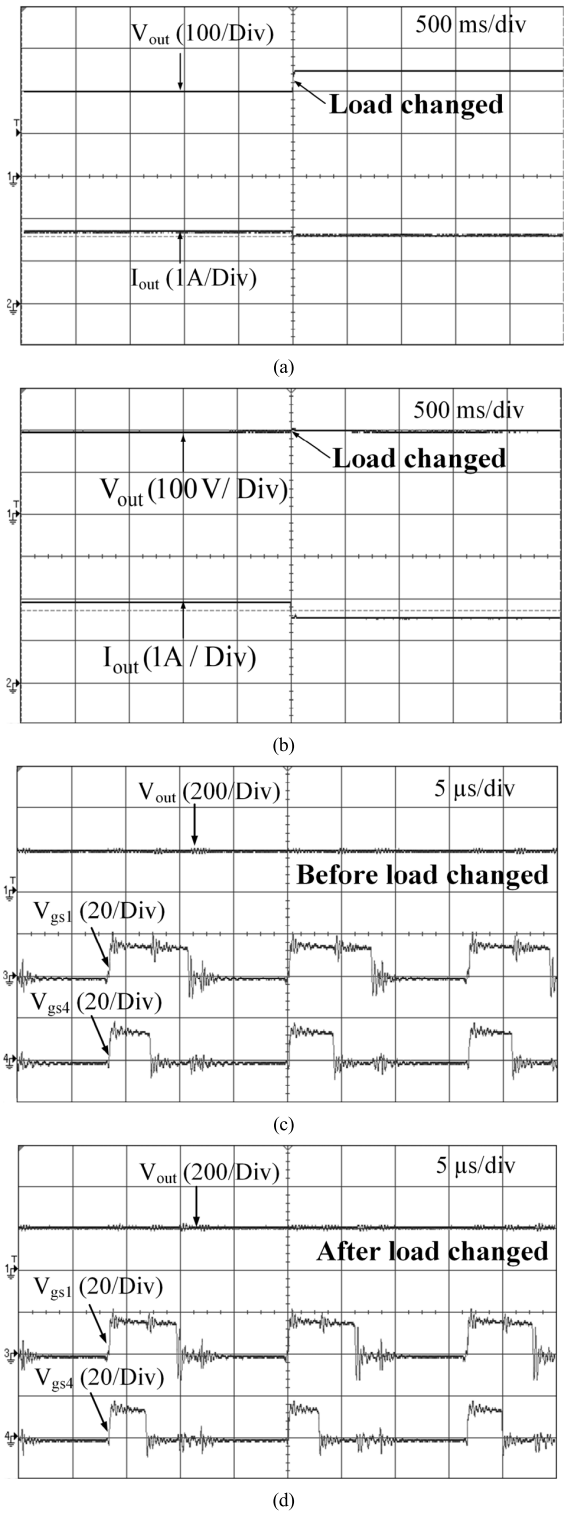

FIGURE 20. Experimental results of the output voltage regulation under load change: (a) Without the output voltage regulation (b) With the output voltage regulation (c) The output voltage and duty cycle of gating signals before load changed (d) The output voltage and duty cycle of gating signals after load changed.

Figure 17(b) with the Tx coils 1 and 4 are excited. The reference output voltage is at 200 V. At the beginning, the load resistance is set to 120 Ω, then it is instantly stepped up to 150 Ω. Without the voltage regulation, the output voltage is increased from 200 to 250 V, as shown in Figure 20 (a). This is due to the duty cycle of both excitation switch S_1 and S_4 are fixed. With the proposed control, the output voltage can

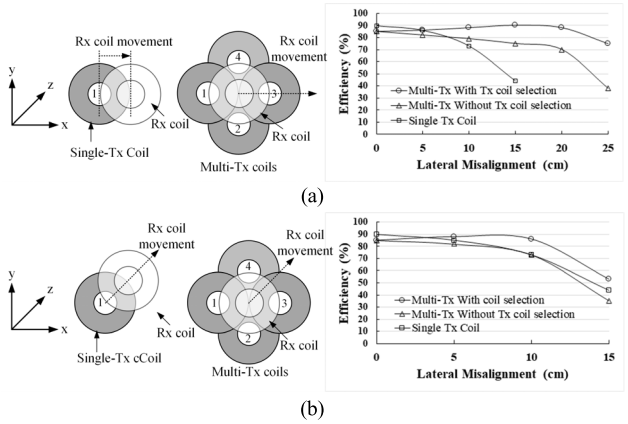

FIGURE 21. Measured system efficiency: (a) Receiver coil movement along a horizontal direction; (b) Receiver coil movement along direction between transmitter coil 4 and 3.

be maintained at 200 V, as shown in Figure 20 (b). During the output voltage regulation process, the gate signals of switches S_1 and S_4 (V_{gs1} and V_{gs4}) are measured as shown in Figure 20 (c) and (d), respectively. In Figure 20 (c), before the load change is applied, the measured duty cycle of the switches S_1 and S_4 are at 45% and 25.9%, respectively. Once the load change is applied, the duty cycle of switches S_1 and S_4 are reduced to 37% and 16%, respectively, to reduce the output voltage to the reference value.

The system efficiency is experimentally measured when the receiver coil is moved toward the Tx coil 3 and toward both Tx coils 3 and 4, as shown in Figure 21(a) and (b), respectively. The load resistance is fixed at 100 Ω. The system efficiency of the multi-coil WPT system with and without the proposed transmitter coil selection are compared. Without the transmitter coil selection, all transmitter coils are energized. At zero misalignment or at the center of the multi-transmitter coil pad shown in Figure 17(a), the measured efficiencies are at 85% for both cases, because the number of activated transmitter coils are identical. In Figure 21(a), when the misalignment is increased, the measured efficiency of the system without the proposed transmitter coil selection is reduced to 70% and 38% at 20 and 25 cm, respectively. On the other hand, with the proposed transmitter-coil selection method, the measured efficiency is increased to 90% at 15-cm location and decreases to 88% and 75% at 20 and 25 cm, respectively. When the receiver moves toward coils 3 and 4, the system efficiency has been improved from 73% to 86% and 35% to 53% at 10-cm and 15-cm receiver locations, respectively. The measured efficiency of the single Tx coil system is also illustrated in Figure 21(a) and (b). The measured results are in accordance with the simulation shown in Figure 4. At the aligned position (zero-misalignment), the efficiency of a single Tx-coil system is 89.8%, while the multi-coil system efficiency is 85.0%, due to higher coupling coefficient. When the lateral misalignment is increased, the efficiency of the single Tx-coil system is drastically decreased. As shown in Figure 21 (a), at 15-cm misalignment in the horizontal direction, the single-Tx coil efficiency is reduced to 44%, compared with 90% and 75% of the muti-Tx with and without coil selection implementation, respectively. On the other hand, when the misalignment is in the z direction, the efficiency of the muti-Tx coil system becomes close to the single-Tx coil system. The multi-Tx coil configuration with the coil selection offers the highest efficiency at 53% while the efficiency is reduced to 35% if the coil selection procedure is not performed.

IX. CONCLUSION

An improved inverter topology for driving multi-coils SWPT system is presented in this paper, with the aim to reduce component count, cost, size, and complexity of the conventional excitation circuits. Only (n+1) power switches for n transmitter coils are required. The dc output voltage is regulated through the transmitter-side control by adjusting the duty cycle of the gate signals of the excited switches. The current in each transmitter coil can be independently controlled where the proper current sharing is possible. The method to select the proper transmitter coil to be excited with respect to the receiver coil position is introduced. The principle is based on the comparison of transmitter currents with the predetermined boundary current. With the proposed method, the system efficiency of 90% has been achieved. Experimental results of the created 500-watt system prototype with four transmitter coils and a single receiver coil validate the proposed method.

REFERENCES

[1] C. Liu, C. Jiang, J. Song, and K. T. Chau, "An effective sandwiched wireless power transfer system for charging implantable cardiac pacemaker," *IEEE Trans. Ind. Electron.*, vol. 66, no. 5, pp. 4108–4117, May 2019.
[2] C. Jiang, K. T. Chau, Y. Y. Leung, C. Liu, C. H. T. Lee, and W. Han, "Design and analysis of wireless ballastless fluorescent lighting," *IEEE Trans. Ind. Electron.*, vol. 66, no. 5, pp. 4065–4074, May 2019.
[3] Y. Jang and M. M. Jovanovic, "A contactless electrical energy transmission system for portable-telephone battery chargers," *IEEE Trans. Ind. Electron.*, vol. 50, no. 3, pp. 520–527, Jun. 2003.
[4] S. Nutwong, A. Sangswang, S. Naetiladdanon, and E. Mujjalinvimut, "A novel output power control of wireless powering kitchen appliance system with free-positioning feature," *Energies*, vol. 11, no. 7, p. 1671, Jun. 2018.
[5] C. Cai, J. Wang, Z. Fang, P. Zhang, M. Hu, J. Zhang, L. Li, and Z. Lin, "Design and optimization of load-independent magnetic resonant wireless charging system for electric vehicles," *IEEE Access*, vol. 6, pp. 17264–17274, 2018.
[6] K. Aditya, V. K. Sood, and S. S. Williamson, "Magnetic characterization of unsymmetrical coil pairs using Archimedean spirals for wider misalignment tolerance in IPT systems," *IEEE Trans. Transport. Electrific.*, vol. 3, no. 2, pp. 454–463, Jun. 2017.
[7] M. Budhia, G. A. Covic, and J. T. Boys, "Design and optimization of circular magnetic structures for lumped inductive power transfer systems," *IEEE Trans. Power Electron.*, vol. 26, no. 11, pp. 3096–3108, Nov. 2011.
[8] A. P. Sample, D. T. Meyer, and J. R. Smith, "Analysis, experimental results, and range adaptation of magnetically coupled resonators for wireless power transfer," *IEEE Trans. Ind. Electron.*, vol. 58, no. 2, pp. 544–554, Feb. 2011.
[9] M. Moghaddami, A. Sundararajan, and A. I. Sarwat, "A power-frequency controller with resonance frequency tracking capability for inductive power transfer systems," *IEEE Trans. Ind. Appl.*, vol. 54, no. 2, pp. 1773–1783, Mar. 2018.
[10] Y. Jiang, L. Wang, Y. Wang, M. Wu, Z. Zeng, Y. Liu, and J. Sun, "Phase-locked loop combined with chained trigger mode used for impedance matching in wireless high power transfer," *IEEE Trans. Power Electron.*, vol. 35, no. 4, pp. 4272–4285, Apr. 2020.

[11] Y. Lim, H. Tang, S. Lim, and J. Park, "An adaptive impedance-matching network based on a novel capacitor matrix for wireless power transfer," *IEEE Trans. Power Electron.*, vol. 29, no. 8, pp. 4403–4413, Aug. 2014.

[12] Z. Zhang, W. Ai, Z. Liang, and J. Wang, "Topology-reconfigurable capacitor matrix for encrypted dynamic wireless charging of electric vehicles," *IEEE Trans. Veh. Technol.*, vol. 67, no. 10, pp. 9284–9293, Oct. 2018.

[13] H. Feng, T. Cai, S. Duan, J. Zhao, X. Zhang, and C. Chen, "An LCC-compensated resonant converter optimized for robust reaction to large coupling variation in dynamic wireless power transfer," *IEEE Trans. Ind. Electron.*, vol. 63, no. 10, pp. 6591–6601, Oct. 2016.

[14] F. Lu, H. Zhang, H. Hofmann, W. Su, and C. C. Mi, "A dual-coupled LCC-compensated IPT system with a compact magnetic coupler," *IEEE Trans. Power Electron.*, vol. 33, no. 7, pp. 6391–6402, Jul. 2018.

[15] H. Feng, T. Cai, S. Duan, X. Zhang, H. Hu, and J. Niu, "A dual-side-detuned series–series compensated resonant converter for wide charging region in a wireless power transfer system," *IEEE Trans. Ind. Electron.*, vol. 65, no. 3, pp. 2177–2188, Mar. 2018.

[16] H. Li, J. Li, K. Wang, W. Chen, and X. Yang, "A maximum efficiency point tracking control scheme for wireless power transfer systems using magnetic resonant coupling," *IEEE Trans. Power Electron.*, vol. 30, no. 7, pp. 3998–4008, Jul. 2015.

[17] W. X. Zhong and S. Y. R. Hui, "Maximum energy efficiency tracking for wireless power transfer systems," *IEEE Trans. Power Electron.*, vol. 30, no. 7, pp. 4025–4034, Jul. 2015.

[18] X. Mou, O. Groling, and H. Sun, "Energy-efficient and adaptive design for wireless power transfer in electric vehicles," *IEEE Trans. Ind. Electron.*, vol. 64, no. 9, pp. 7250–7260, Sep. 2017.

[19] S. Kim, G. A. Covic, and J. T. Boys, "Tripolar pad for inductive power transfer systems for EV charging," *IEEE Trans. Power Electron.*, vol. 32, no. 7, pp. 5045–5057, Jul. 2017.

[20] M. Pathmanathan, S. Nie, N. Yakop, and P. W. Lehn, "Field-oriented control of a three-phase wireless power transfer system transmitter," *IEEE Trans. Transport. Electrific.*, vol. 5, no. 4, pp. 1015–1026, Dec. 2019.

[21] Z. Yan, B. Yang, H. Liu, C. Chen, M. Waqas, R. Mai, and Z. He, "Efficiency improvement of wireless power transfer based on multitransmitter system," *IEEE Trans. Power Electron.*, vol. 35, no. 9, pp. 9011–9023, Sep. 2020.

[22] X. Liu, W. Han, C. Liu, and P. W. T. Pong, "Marker-free coil-misalignment detection approach using TMR sensor array for dynamic wireless charging of electric vehicles," *IEEE Trans. Magn.*, vol. 54, no. 11, pp. 1–5, Nov. 2018.

[23] W. Han, K. T. Chau, C. Jiang, and W. Liu, "Accurate position detection in wireless power transfer using magnetoresistive sensors for implant applications," *IEEE Trans. Magn.*, vol. 54, no. 11, pp. 1–5, Nov. 2018.

[24] W. Ni, I. B. Collings, X. Wang, R. P. Liu, A. Kajan, M. Hedley, and M. Abolhasan, "Radio alignment for inductive charging of electric vehicles," *IEEE Trans. Ind. Informat.*, vol. 11, no. 2, pp. 427–440, Apr. 2015.

[25] A. Azad, A. Echols, V. Kulyukin, R. Zane, and Z. Pantic, "Analysis, optimization, and demonstration of a vehicular detection system intended for dynamic wireless charging applications," *IEEE Trans. Transport. Electrific.*, vol. 5, no. 1, pp. 147–161, Mar. 2019.

[26] S. Y. Jeong, H. G. Kwak, G. C. Jang, S. Y. Choi, and C. T. Rim, "Dual-purpose nonoverlapping coil sets as metal object and vehicle position detections for wireless stationary EV chargers," *IEEE Trans. Power Electron.*, vol. 33, no. 9, pp. 7387–7397, Sep. 2018.

[27] A. Babu and B. George, "Sensor system to aid the vehicle alignment for inductive EV chargers," *IEEE Trans. Ind. Electron.*, vol. 66, no. 9, pp. 7338–7346, Sep. 2019.

[28] N. Hatchavanich, A. Sangswang, and M. Konghirun, "Secondary-side voltage control via primary-side controller for wireless EV chargers," *IEEE Access*, vol. 8, pp. 203543–203554, 2020.

[29] T.-S. Lee, S.-J. Huang, S.-H. Dai, and J.-L. Su, "Design of misalignment-insensitive inductive power transfer via interoperable coil module and dynamic power control," *IEEE Trans. Power Electron.*, vol. 35, no. 9, pp. 9024–9033, Sep. 2020.

[30] X. Dai, J. Jiang, Y. Li, and T. Yang, "A phase-shifted control for wireless power transfer system by using dual excitation units," *Energies*, vol. 10, no. 7, p. 1000, Jul. 2017.

[31] A. T. L. Lee, W. Jin, S.-C. Tan, and S. Y. Hui, "Buck-boost single-inductor multiple-output high-frequency inverters for medium-power wireless power transfer," *IEEE Trans. Power Electron.*, vol. 34, no. 4, pp. 3457–3473, Apr. 2019.

[32] S. Nutwong, A. Sangswang, and S. Naetiladdanon, "An inverter topology for wireless power transfer system with multiple transmitter coils," *Appl. Sci.*, vol. 9, no. 8, p. 1551, Apr. 2019.

[33] *Qi System Description: Wireless Power Transfer, Volume I: Low Power, Part 1: Interface Definition, Version 1.1*, Wireless Power Consortium, Piscataway, NJ, USA, Apr. 2012.

[34] N. Sato, H. Kifune, and S. Komeda, "A coil layout of wireless power transfer systems based on multicoil arrangement for underwater vehicles," *Electr. Eng. Jpn.*, vol. 207, no. 2, pp. 38–48, Apr. 2019.

[35] *Wireless Power Transfer for Light-Duty Plug-In/Electric Vehicles and Alignment Methodology*, Standard SAEJ2954, May 2016. [Online]. Available: http://standards.sae.org/j2954_201605/

[36] ICNIRP, "Guidelines for limiting exposure to time -varying electric and magnetic fields (1 Hz to 100 kHz)," *Health Phys.*, vol. 99, no. 6, pp. 818–836, 2010.

[37] R. L. Steigerwald, "A comparison of half-bridge resonant converter topologies," *IEEE Trans. Power Electron.*, vol. 3, no. 2, pp. 174–182, Apr. 1988.

EKKACHAI CHAIDEE (Member, IEEE) received the B.Sc.Ind.Ed. degree in electrical engineering from the King Mongkut's University of Technology Thonburi (KMUTT), Bangkok, Thailand, in 2001, and the M.Sc. (Eng.) degree in electrical engineering from the King Mongkut's University of Technology North Bangkok (KMUTNB), Bangkok, Thailand, in 2008. He is currently pursuing the D.Eng. degree in electrical and information engineering technology with KMUTT. His current research interests include the resonant inverter and control technique for wireless power transfer.

ANAWACH SANGSWANG (Member, IEEE) was born in Bangkok, Thailand. He received the B.Eng. degree from the King Mongkut's University of Technology Thonburi (KMUTT), Bangkok, in 1995, and the M.S. and Ph.D. degrees in electrical engineering from Drexel University, Philadelphia, PA, USA, in 1999 and 2003, respectively. From 1999 to 2003, he was a Research Assistant with the Center for Electric Power Engineering, Drexel University. Since 2006, he has been an Assistant Professor with the Department of Electrical Engineering, KMUTT. His research interests include induction heating, wireless power transfer, energy management systems, and power system stability.

SUMATE NAETILADDANON (Member, IEEE) received the B.Eng. degree from Chulalongkorn University, Bangkok, Thailand, in 1995, the M.Sc. degree from the Rensselaer Polytechnic Institute, Troy, NY, USA, in 1999, and the Ph.D. degree from Osaka University, Osaka, Japan, in 2006. He is currently an Assistant Professor with the Department of Electrical Engineering, King Mongkut's University of Technology Thonburi (KMUTT), Bangkok. His current research interests include smart grid technologies, large-scale renewable power integration to the grid, smart power electronics for energy efficiency, and renewable energy applications and systems.

SUPAPONG NUTWONG received the B.Eng. and M.Eng. degrees in electrical engineering and the D.Eng. degree in electrical and information engineering technology from the King Mongkut's University of Technology Thonburi (KMUTT), Bangkok, Thailand, in 2007, 2011, and 2019, respectively. Since 2020, he has been a Lecturer with the Department of Electrical Engineering, KMUTT. His current research interests include power electronics and control for wireless power transfer (WPT) systems and induction heating (IH) applications.